

Modified steady discrete unified gas kinetic scheme for multiscale radiative heat transfer

Xinliang Song^a, Yue Zhang^a, Xiaofeng Zhou^{c,*}, Chuang Zhang^d, Zhaoli Guo^{b,*}

^a*State Key Laboratory of Coal Combustion, School of Energy and Power Engineering, Huazhong University of Science and Technology, Wuhan 430074, China*

^b*Institute of Interdisciplinary Research for Mathematics and Applied Science, Huazhong University of Science and Technology, Wuhan 430074, China*

^c*Department of Nuclear Engineering and Technology, School of Energy and Power Engineering, Huazhong University of Science and Technology, Wuhan 430074, China*

^d*Department of Mechanics and Aerospace Engineering, Southern University of Science and Technology, Shenzhen 518055, China*

Abstract

In this work, a steady discrete unified gas kinetic scheme (SDUGKS) is proposed to solve the steady radiative transfer equation (RTE), which is an improvement of the original SDUGKS [X. F. Zhou *et al.*, *J. Comput. Phys.* 423, 109767 (2020)]. The trapezoidal rule other than the rectangular rule used in the original SDUGKS is adopted in the proposed method in the reconstruction of energy flux across cell interface, just as the unsteady DUGKS. By this way, the characteristic line length of the modified SDUGKS establishes a relationship with the Courant-Friedrichs-Lewy (CFL) number in the DUGKS, which guarantees the accuracy of the modified SDUGKS. Furthermore, the characteristic line length is no longer limited by the extinction coefficient like in original SDUGKS. As a result, the modified SDUGKS is more accurate and robust than original SDUGKS, and more efficient than the DUGKS for steady radiation problems. Furthermore, the smooth linear interpolation and the van Leer limiter are used for problems with smooth and discontinuous optical thicknesses, respectively. Several numerical tests with optical thickness varying from optical thin to thick are conducted to validate the present scheme. Numerical results demonstrate that the modified SDUGKS can serve as an effective tool in the study of multiscale steady radiative heat transfer in participating media.

Keywords: Steady radiative heat transfer, Steady discrete unified gas kinetic scheme, van Leer limiter

1. Introduction

Radiative heat transfer appears in many research fields and engineering applications such as combustion systems [1, 2], solar radiation [3, 4], nuclear reactor physics [5], atmospheric radiation [6, 7], radiative hypersonic flows [8, 9], fluorescence imaging [10] and other processes. Most of these problems involve a wide range of optical thicknesses. Since the velocity of photon is about 3×10^8 m/s, it is reasonable to ignore the

*Corresponding author

Email addresses: zhouxiaofeng@hust.edu.cn (Xiaofeng Zhou), zlguo@mail.hust.edu.cn (Zhaoli Guo)

transient component and only consider the steady behaviors [11, 12]. Traditionally, the diffusion equation (DE) which describes the radiative heat transfer at the macroscopic scale is an efficient way for optical thick problems, but it becomes invalid for problems involving optical thin regions [13]. On the contrary, the photon transport equation, or radiative transfer equation (RTE), can be employed to describe radiative process for all optical thickness. However, as a high dimensional integral-differential equation, it is a challenging task to develop efficient numerical schemes with the capability of solving the RTE in all regimes.

In the past few decades, a number of numerical methods have been developed to solve the RTE, such as Monte Carlo method (MCM) [14, 15], discrete ordinate method (DOM) [16, 17], finite element method (FEM) [18], finite volume method (FVM) [19, 20], spectral element method [21], zonal method [22], discrete transfer method (DTM) [23, 24], and DRESOR method [25, 26]. Several recent reviews are also available [12, 27, 28]. Among those methods, the MCM, as a powerful and robust probabilistic approach, has achieved great success. However, the method is computationally expensive for participating media with large optical thickness where a great number of photon bundles need to be traced to decrease the statistic errors [29]. Similarly, the deterministic DOM, FEM and FVM also become inefficient when encountering optical thick media, because the cell size of these methods is also limited by the photon mean free path (MFP). For instance, the diamond difference (DD) method, a popular DOM, usually suffers from nonphysical oscillations in optical thick media unless the mesh is fine enough. In order to solve multiscale radiative transfer problems accurately and efficiently, some robust methods have been proposed. A common strategy is using the domain decomposition technique, in which the domain is decomposed into mesoscopic and macroscopic subdomains [10, 30]. However, such method faces a critical problem in finding the coupling rule between the mesoscopic and the macroscopic subdomains. Usually, a buffer zone between two neighboring decomposed domains is adopted [31]. Unfortunately, the solution of the coupled system in the buffer zone may be not easy [32]. An alternative method for multiscale problem is to solve the RTE in a unified approach, such as the unified gas kinetic scheme (UGKS) [33, 34] and the discrete unified gas kinetic scheme (DUGKS) [35, 36]. Comparing with the domain decomposition method, the unified methods avoid the coupling of different subdomains. By considering the photon transport and collision simultaneously, these two methods have been applied efficiently and accurately to a series of transient multiscale radiative transfer problems [37, 38, 39, 40, 41] without requiring the cell size smaller than the photon MFP. However, both UGKS and DUGKS are mainly designed for transient problems. Recently, the DUGKS has been extended to solve steady multiscale neutron transfer problems [42], and the numerical results showed that the steady DUGKS (SDUGKS) can achieve a good acceleration compared with the DUGKS for steady multiscale neutron transfer problems. However, a rectangular rule was used in the SDUGKS to reconstruct the interface angular flux. As a result, the method may be not accurate enough especially for optical thick problem with coarse mesh. In addition, the key parameter characteristic line length is strictly restricted by the cell size and the extinction coefficient.

In this work, a modified steady discrete unified gas kinetic scheme is proposed for steady multiscale

radiative heat transfer problems. Similar to the DUGKS, a trapezoidal rule is used in the reconstruction of interface angular flux. Therefore, the characteristic line length establishes a subtle connection with the Courant-Friedrichs-Lewy (CFL) number in DUGKS to ensure the same accuracy. Consequently, the characteristic line length of the present scheme is only limited by the cell size and no longer restricted by the extinction coefficient. In order to distinguish the two kinds of steady DUGKS, the scheme developed in [42] is remarked as the R-SDUGKS, and the scheme proposed in the present work is denoted as T-SDUGKS.

The remainder of this paper is organized as follows. Section 2 introduces the steady gray radiative transfer equation. The T-SDUGKS for steady gray radiative transfer equation is given in Section 3. Numerical results and discussions are presented in Section 4. Finally, Section 5 gives a brief summary.

2. Steady gray radiative transfer equation

The steady gray radiative transfer equation can be written as [12]

$$\mathbf{s} \cdot \nabla I(\mathbf{x}, \mathbf{s}) = -\beta(\mathbf{x}) I(\mathbf{x}, \mathbf{s}) + \beta(\mathbf{x}) S(\mathbf{x}, \mathbf{s}), \quad (1)$$

$$S(\mathbf{x}, \mathbf{s}) = (1 - \omega(\mathbf{x})) I_b(\mathbf{x}) + \frac{\omega(\mathbf{x})}{4\pi} \int_{4\pi} I(\mathbf{x}, \mathbf{s}') d\Omega', \quad (2)$$

where $I(\mathbf{x}, \mathbf{s})$ is the radiation intensity at position \mathbf{x} and direction \mathbf{s} , $\beta(\mathbf{x})$ is the extinction coefficient related to the local photon mean free path (λ) as $\lambda = 1/\beta$, $S(\mathbf{x}, \mathbf{s})$ is the source term of the RTE, $\omega(\mathbf{x})$ is the scattering albedo, $I_b(\mathbf{x})$ is the blackbody intensity, and Ω' is the corresponding solid angle. For equilibrium problems, the blackbody intensity can be calculated according to energy conservation

$$I_b(\mathbf{x}) = \frac{1}{4\pi} \int_{4\pi} I(\mathbf{x}, \mathbf{s}) d\Omega. \quad (3)$$

For nonequilibrium problems with a given temperature field of the medium, the blackbody intensity can be calculated by the Stefan-Boltzmann law [12],

$$I_b(\mathbf{x}) = \frac{\sigma T^4(\mathbf{x})}{\pi}, \quad (4)$$

where σ is the Stefan-Boltzmann constant and $T(\mathbf{x})$ is the local temperature of the medium.

In radiative heat transfer problems, the local incident radiation energy G and heat flux \mathbf{q} can be determined by,

$$G(\mathbf{x}) = \int_{4\pi} I(\mathbf{x}, \mathbf{s}) d\Omega, \quad (5)$$

$$\mathbf{q}(\mathbf{x}) = \int_{4\pi} I(\mathbf{x}, \mathbf{s}) \mathbf{s} d\Omega. \quad (6)$$

3. T-SDUGKS for steady radiative transfer equation

3.1. Discretization of steady radiative transfer equation

In order to numerically solve the RTE, Eqs. (1) and (2) are first discretized in physical and solid angle spaces. The continuous physical space is divided into a set of cells with the finite volume scheme. The

solid angle is discretized into M discrete angles using certain quadrature rules, such as Gauss-Legendre quadrature, Gauss-Chebyshev quadrature, and S_N quadrature. Then the corresponding discrete forms can be written as

$$\frac{1}{V_j} \sum_f (\mathbf{s}_k \cdot \mathbf{n}_f) I(\mathbf{x}_f, \mathbf{s}_k) \Delta S_f = -\beta(\mathbf{x}_j) I(\mathbf{x}_j, \mathbf{s}_k) + \beta(\mathbf{x}_j) S(\mathbf{x}_j, \mathbf{s}_k), \quad (7)$$

$$S(\mathbf{x}_j, \mathbf{s}_k) = (1 - \omega(\mathbf{x}_j)) I_b(\mathbf{x}_j) + \frac{\omega(\mathbf{x}_j)}{4\pi} \sum_{m=1}^M I(\mathbf{x}_j, \mathbf{s}'_m) \omega_m, \quad (8)$$

where $I(\mathbf{x}_j, \mathbf{s}_k)$ denotes the cell averaged radiation intensity in the control volume V_j centered at \mathbf{x}_j along the photon propagation direction \mathbf{s}_k , \mathbf{n}_f is the outward unit normal vector at the interface \mathbf{x}_f , ΔS_f is the corresponding interface area, and ω_m and \mathbf{s}'_m are the weight and discrete angle of the corresponding spherical quadrature, respectively.

3.2. Reconstruction of the interface radiation intensity

To update the radiation intensity $I(\mathbf{x}_j, \mathbf{s}_k)$, the reconstruction of the interface intensity $I(\mathbf{x}_f, \mathbf{s}_k)$ becomes the key point. By integrating Eq. (7) along the direction \mathbf{s}_k with a certain length l and applying the trapezoidal rule to the right hand term, one can obtain

$$\begin{aligned} \frac{I(\mathbf{x}_f, \mathbf{s}_k) - I(\mathbf{x}_f - l\mathbf{s}_k, \mathbf{s}_k)}{l} = \\ \frac{\beta(\mathbf{x}_f)}{2} [S(\mathbf{x}_f, \mathbf{s}_k) - I(\mathbf{x}_f, \mathbf{s}_k)] + \frac{\beta(\mathbf{x}_f - l\mathbf{s}_k)}{2} [S(\mathbf{x}_f - l\mathbf{s}_k, \mathbf{s}_k) - I(\mathbf{x}_f - l\mathbf{s}_k, \mathbf{s}_k)], \end{aligned} \quad (9)$$

where both the transport and collision terms are coupled simultaneously. We note that the rectangular rule is used in the R-SDUGKS [42]. By reviewing the interface radiation intensity in transient radiative heat transfer, the relationship between the characteristic line length in Eq. (9) and the CFL used in Ref. [39] can be easily established as

$$l = \frac{1}{2} \alpha \Delta x_{min}, \quad (10)$$

where $0 < \alpha < 1$ is the CFL number and Δx_{min} is the minimal mesh size. It is obvious that the characteristic line length is no longer limited by the maximal extinction coefficient as mentioned in Ref. [42].

In order to remove the implicit term of Eq. (9), two new distribution functions are introduced,

$$\bar{I}^+(\mathbf{x}, \mathbf{s}) = I(\mathbf{x}, \mathbf{s}) - \frac{\beta(\mathbf{x})l}{2} (I(\mathbf{x}, \mathbf{s}) - S(\mathbf{x}, \mathbf{s})), \quad (11)$$

$$\bar{I}(\mathbf{x}, \mathbf{s}) = I(\mathbf{x}, \mathbf{s}) + \frac{\beta(\mathbf{x})l}{2} (I(\mathbf{x}, \mathbf{s}) - S(\mathbf{x}, \mathbf{s})). \quad (12)$$

Substituting Eqs. (11) and (12) into Eq. (9), one can obtain

$$\bar{I}(\mathbf{x}_f, \mathbf{s}_k) = \bar{I}^+(\mathbf{x}_f - l\mathbf{s}_k, \mathbf{s}_k). \quad (13)$$

For smooth problems, $\bar{I}^+(\mathbf{x}_f - l\mathbf{s}_k, \mathbf{s}_k)$ can be approximated as

$$\bar{I}^+(\mathbf{x}_f - l\mathbf{s}_k, \mathbf{s}_k) = \bar{I}^+(\mathbf{x}_f, \mathbf{s}_k) - l\mathbf{s}_k \cdot \boldsymbol{\sigma}_f, \quad (14)$$

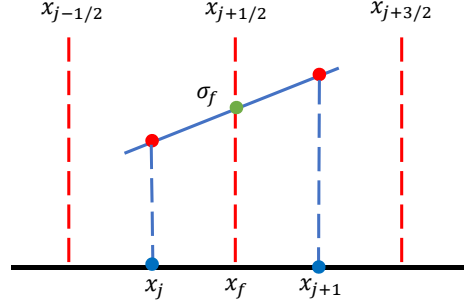


Figure 1: Schematic of one-dimensional cell geometry for smooth problems.

where $\bar{I}^+(\mathbf{x}_f, \mathbf{s}_k)$ and the gradient $\sigma_f = \nabla \bar{I}^+(\mathbf{x}_f, \mathbf{s}_k)$ at the cell interface can be approximated by smooth linear interpolation [35]. As an example, figure 1 shows the one-dimensional (1D) case. In this case, the reconstructions become

$$\sigma_{j+1/2} = \frac{\bar{I}^+(x_{j+1}, \mu_k) - \bar{I}^+(x_j, \mu_k)}{x_{j+1} - x_j}, \quad (15)$$

$$\bar{I}^+(x_{j+1/2}, \mu_k) = \bar{I}^+(x_j, \mu_k) + \sigma_{j+1/2} (x_{j+1/2} - x_j), \quad (16)$$

where μ_k is the direction cosine of \mathbf{s}_k along x direction. For discontinuous problems, the van Leer limiter [43] can be adopted to reconstruct the gradient in each cell. Assuming that $\bar{I}^+(\mathbf{x}_j, \mathbf{s}_k)$ is linear in cell V_j , then $\bar{I}^+(\mathbf{x}_f - l\mathbf{s}_k, \mathbf{s}_k)$ can be reconstructed as

$$\bar{I}^+(\mathbf{x}_f - l\mathbf{s}_k, \mathbf{s}_k) = \bar{I}^+(\mathbf{x}_j, \mathbf{s}_k) + (\mathbf{x}_f - l\mathbf{s}_k - \mathbf{x}_j) \cdot \sigma_j, (\mathbf{x}_f - l\mathbf{s}_k) \in V_j, \quad (17)$$

where σ_j is the slope of \bar{I}^+ in cell j . For example, in the 1D case shown in Fig. 2, the variable $\bar{I}^+(x_f - l\mu_k, \mu_k)$

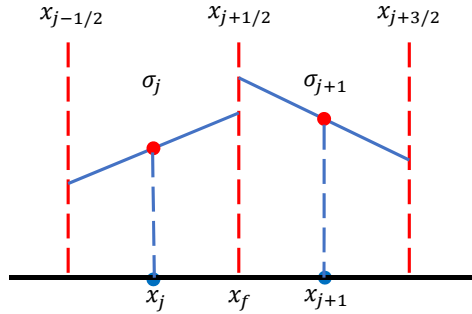


Figure 2: Schematic of one-dimensional cell geometry for discontinuous problems.

can be approximated as

$$\bar{I}^+(x_f - l\mu_k, \mu_k) = \begin{cases} \bar{I}^+(x_j, \mu_k) + (x_f - l\mu_k - x_j) \sigma_j, & \mu_k > 0, \\ \bar{I}^+(x_{j+1}, \mu_k) + (x_f - l\mu_k - x_{j+1}) \sigma_{j+1}, & \mu_k < 0. \end{cases} \quad (18)$$

The reconstruction of σ_j in each cell becomes

$$\sigma_j = [\text{sgn}(a_1) + \text{sgn}(a_2)] \frac{|a_1| |a_2|}{|a_1| + |a_2|}, \quad (19)$$

where

$$a_1 = \frac{\bar{I}^+(x_j, \mu_k) - \bar{I}^+(x_{j-1}, \mu_k)}{x_j - x_{j-1}}, a_2 = \frac{\bar{I}^+(x_{j+1}, \mu_k) - \bar{I}^+(x_j, \mu_k)}{x_{j+1} - x_j}. \quad (20)$$

Then $\bar{I}(\mathbf{x}_f, \mathbf{s}_k)$ can be obtained from Eq. (13).

Next, integrating Eq. (12) over the entire solid angle, one can obtain

$$\int_{4\pi} I(\mathbf{x}, \mathbf{s}) d\Omega = \frac{2}{2 + \beta(\mathbf{x})(1 - \omega(\mathbf{x}))l} \int_{4\pi} \bar{I}(\mathbf{x}, \mathbf{s}) d\Omega + \frac{4\pi\beta(\mathbf{x})(1 - \omega(\mathbf{x}))l}{2 + \beta(\mathbf{x})(1 - \omega(\mathbf{x}))l} I_b(\mathbf{x}). \quad (21)$$

Then from Eq. (12), the radiation intensity at the cell interface can be computed by

$$\begin{aligned} I(\mathbf{x}_f, \mathbf{s}_k) &= \frac{2}{2 + \beta(\mathbf{x}_f)l} \bar{I}(\mathbf{x}_f, \mathbf{s}_k) + \frac{\beta(\mathbf{x}_f)(1 - \omega(\mathbf{x}_f))l}{2 + \beta(\mathbf{x}_f)(1 - \omega(\mathbf{x}_f))l} I_b(\mathbf{x}_f) \\ &+ \frac{2\beta(\mathbf{x}_f)\omega(\mathbf{x}_f)l}{(2 + \beta(\mathbf{x}_f)l)[2 + \beta(\mathbf{x}_f)(1 - \omega(\mathbf{x}_f))l]} \frac{1}{4\pi} \sum_{m=1}^M \bar{I}(\mathbf{x}_f, \mathbf{s}'_m) \omega_m. \end{aligned} \quad (22)$$

3.3. Implicit delta formulation

With the known interface intensity $I(\mathbf{x}_f, \mathbf{s}_k)$, the implicit delta formulation method will be used to update the cell center intensity $I(\mathbf{x}_j, \mathbf{s}_k)$. First, Eq. (7) is solved using the following iterative scheme

$$\frac{1}{V_j} \sum_f (\mathbf{s}_k \cdot \mathbf{n}_f) I^{n+1}(\mathbf{x}_f, \mathbf{s}_k) \Delta S_f = -\beta(\mathbf{x}_j) I^{n+1}(\mathbf{x}_j, \mathbf{s}_k) + \beta(\mathbf{x}_j) S^n(\mathbf{x}_j, \mathbf{s}_k), \quad (23)$$

with

$$S^n(\mathbf{x}_j, \mathbf{s}_k) = (1 - \omega(\mathbf{x}_j)) I_b^n(\mathbf{x}_j) + \frac{\omega(\mathbf{x}_j)}{4\pi} \sum_{m=1}^M I^n(\mathbf{x}_j, \mathbf{s}'_m) \omega_m. \quad (24)$$

where n represents the n -th iteration step. If we define the increment between two successive iterations as

$$\Delta I^n(\mathbf{x}, \mathbf{s}) = I^{n+1}(\mathbf{x}, \mathbf{s}) - I^n(\mathbf{x}, \mathbf{s}). \quad (25)$$

Then Eq. (23) can be rewritten in the delta form,

$$\frac{1}{V_j} \sum_f (\mathbf{s}_k \cdot \mathbf{n}_f) \Delta I^n(\mathbf{x}_f, \mathbf{s}_k) \Delta S_f + \beta(\mathbf{x}_j) \Delta I^n(\mathbf{x}_j, \mathbf{s}_k) = Res^n(\mathbf{x}_j, \mathbf{s}_k), \quad (26)$$

where $Res^n(\mathbf{x}_j, \mathbf{s}_k)$ is the residual,

$$Res^n(\mathbf{x}_j, \mathbf{s}_k) = \beta(\mathbf{x}_j) S^n(\mathbf{x}_j, \mathbf{s}_k) - \beta(\mathbf{x}_j) I^n(\mathbf{x}_j, \mathbf{s}_k) - \frac{1}{V_j} \sum_f (\mathbf{s}_k \cdot \mathbf{n}_f) I^n(\mathbf{x}_f, \mathbf{s}_k) \Delta S_f. \quad (27)$$

Overall, the cell center radiation intensity $I^{n+1}(\mathbf{x}_j, \mathbf{s}_k)$ can be obtained from Eqs. (25) and (26). Once the iteration converges, the increment ΔI^n will vanish, suggesting that the two terms on the left hand side of Eq. (26) dose not affect the converged solution. Particularly, a first-order upwind scheme will be employed to calculate the first term on the left hand side of Eq. (26). The accuracy of the final results are determined by the right-hand term of Eq. (26), and a higher-order scheme should be employed for this term. In the present method, the T-SDUGKS is employed to calculate the interface angular flux, i.e., the last term of Eq. (27).

The one-dimensional case is taken as an example to show the details of solving $I^{n+1}(x_j, \mu_k)$. In this case, Eq. (26) can be written as

$$\frac{1}{V_j} (\mu_k \Delta I^n(x_{j+1/2}, \mu_k) - \mu_k \Delta I^n(x_{j-1/2}, \mu_k)) \Delta S_f + \beta \Delta I^n(x_j, \mu_k) = Res^n(x_j, \mu_k), \quad (28)$$

where the increment of interface intensity is approximated by the upwind scheme, i.e.,

$$\begin{cases} \Delta I^n(x_{j+1/2}, \mu_k) = \Delta I^n(x_j, \mu_k), & \mu_k > 0, \\ \Delta I^n(x_{j-1/2}, \mu_k) = \Delta I^n(x_j, \mu_k), & \mu_k < 0. \end{cases} \quad (29)$$

Substituting Eq. (29) into Eq. (28), the increment $\Delta I^n(x_j, \mu_k)$ can be computed as

$$\Delta I^n(x_j, \mu_k) = \frac{Res^n(x_j, \mu_k) V_j + |\mu_k| \Delta S_f \Delta I^n(x_{in}, \mu_k)}{\beta(x_j) V_j + |\mu_k| \Delta S_f}, \quad (30)$$

where

$$\Delta I^n(x_{in}, \mu_k) = \begin{cases} \Delta I^n(x_{j-1/2}, \mu_k), & \mu_k > 0, \\ \Delta I^n(x_{j+1/2}, \mu_k), & \mu_k < 0. \end{cases} \quad (31)$$

According to Eqs. (25) and (30), the cell center intensity $I^{n+1}(x_j, \mu_k)$ can be updated. The two- and three-dimensional cases are similar and are not presented here.

3.4. Boundary condition

In this work, the diffusively emitting and reflecting boundaries are considered. The general boundary condition for the steady radiative transfer equation can be expressed as

$$I(\mathbf{x}_w, \mathbf{s}_k) = \epsilon_w I_b(\mathbf{x}_w) + \frac{\rho_w}{\pi} \sum_{\mathbf{n}_w \cdot \mathbf{s}'_m < 0} (\mathbf{n}_w \cdot \mathbf{s}'_m) I(\mathbf{x}_w, \mathbf{s}'_m) \omega_m, \mathbf{n}_w \cdot \mathbf{s}_k > 0, \quad (32)$$

where ϵ_w is the diffuse emissivity, ρ_w is the diffuse reflectivity, $\epsilon_w = 1 - \rho_w$, $I_b(\mathbf{x}_w)$ is the blackbody radiation intensity at the boundary surface with a specified temperature, and \mathbf{n}_w is the inner normal vector at the boundary.

3.5. Comparison of the numerical fluxes of R-SDUGKS and T-SDUGKS

We now analyze the differences between the R-SDUGKS and T-SDUGKS. Firstly, it is noted that the exact solution at the cell interface can be expressed as

$$I_{exact}(\mathbf{x}_f, \mathbf{s}_k) - I(\mathbf{x}_f - l\mathbf{s}_k, \mathbf{s}_k) = \int_0^l A(\mathbf{x}_f - l\mathbf{s}_k + h\mathbf{s}_k, \mathbf{s}_k) dh, \quad (33)$$

where

$$A(\mathbf{x}, \mathbf{s}_k) = \frac{\beta(\mathbf{x}) \omega(\mathbf{x})}{4\pi} \sum_{m=1}^M I(\mathbf{x}, \mathbf{s}'_m) \omega_m - \beta(\mathbf{x}) I(\mathbf{x}, \mathbf{s}_k) + \beta(\mathbf{x}) (1 - \omega(\mathbf{x})) I_b(\mathbf{x}). \quad (34)$$

If we approximate the integration in Eq. (33) with the rectangular rule, we will get the R-SDUGKS [42], and Eq. (33) becomes

$$I_{recta}(\mathbf{x}_f, \mathbf{s}_k) - I(\mathbf{x}_f - l\mathbf{s}_k, \mathbf{s}_k) = lA(\mathbf{x}_f - l\mathbf{s}_k, \mathbf{s}_k). \quad (35)$$

On the other hand, the T-SDUGKS will be obtained when the trapezoidal rule is used,

$$I_{trape}(\mathbf{x}_f, \mathbf{s}_k) - I(\mathbf{x}_f - l\mathbf{s}_k, \mathbf{s}_k) = \frac{l}{2} [A(\mathbf{x}_f - l\mathbf{s}_k, \mathbf{s}_k) + A(\mathbf{x}_f, \mathbf{s}_k)]. \quad (36)$$

From Eqs. (33), (35), and (36), we can obtain that

$$I_{recta}(\mathbf{x}_f, \mathbf{s}_k) = I_{exact}(\mathbf{x}_f, \mathbf{s}_k) + O(\Delta x^2) - \frac{l^2}{2} \mathbf{s}_k \cdot \nabla A(\mathbf{x}_f, \mathbf{s}_k) + O(l^3), \quad (37)$$

$$I_{trape}(\mathbf{x}_f, \mathbf{s}_k) = I_{exact}(\mathbf{x}_f, \mathbf{s}_k) + O(\Delta x^2) + \frac{l^3}{12} (\mathbf{s}_k \cdot \nabla)^2 A(\mathbf{x}_f, \mathbf{s}_k) + O(l^4), \quad (38)$$

where the error $O(\Delta x^2)$ comes from the spatial approximation of the second term on the left-hand side of Eqs. (35) or (36). The errors from the quadratures are explicitly expressed in Eqs. (37) or (38) for the two schemes. It can be observed that the approximation error of T-SDUGKS is $O(\Delta x^2) + O(l^3)$ while the R-SDUGKS is $O(\Delta x^2) + O(l^2)$, which means the T-SDUGKS will be more accurate than the R-SDUGKS where $O(l^2)$ cannot be ignored.

3.6. Algorithm

In summary, the iteration procedure of the T-SDUGKS can be summarized as follows:

1. Calculate the interface intensity $I^n(\mathbf{x}_f, \mathbf{s}_k)$.
 - (a) Calculate $\bar{I}^{+,n}(\mathbf{x}_j, \mathbf{s}_k)$ according to Eq. (11).
 - (b) Calculate the distribution function $\bar{I}^n(\mathbf{x}_f, \mathbf{s}_k)$ at cell interface according to Eq. (13).
 - (c) Calculate the interface intensity $I^n(\mathbf{x}_f, \mathbf{s}_k)$ according to Eq. (22).
2. Update the cell center intensity $I^{n+1}(\mathbf{x}_j, \mathbf{s}_k)$.
 - (a) Calculate the residual $Res^n(\mathbf{x}_j, \mathbf{s}_k)$ according to Eqs. (24) and (27).
 - (b) Calculate increments $\Delta I^n(\mathbf{x}_j, \mathbf{s}_k)$ according to Eq. (26).
 - (c) Update the center intensity $I^{n+1}(\mathbf{x}_j, \mathbf{s}_k)$ according to Eq. (25).
3. Repeat step 1 - step 2, until the convergence criteria is satisfied.

When the center intensity is known, the radiation energy $G(\mathbf{x}_j)$ and heat flux $\mathbf{q}(\mathbf{x}_j)$ can be obtained,

$$G(\mathbf{x}_j) = \sum_{k=1}^M I(\mathbf{x}_j, \mathbf{s}_k) \omega_k, \quad (39)$$

$$\mathbf{q}(\mathbf{x}_j) = \sum_{k=1}^M I(\mathbf{x}_j, \mathbf{s}_k) \mathbf{s}_k \omega_k. \quad (40)$$

The convergence criteria in our simulations is defined as

$$E = \frac{\sum_j |G^{n+1}(\mathbf{x}_j) - G^n(\mathbf{x}_j)|}{\sum_j |G^{n+1}(\mathbf{x}_j)|} < 10^{-10}. \quad (41)$$

4. Numerical tests

In this section, several radiative heat transfer problems with the optical thickness ranging from thin to thick regimes are simulated to validate the numerical properties of the proposed T-SDUGKS. In the numerical implementation, the Gauss-Legendre quadrature [44] is adopted to discretize the solid angle with the cosine of zenith $\mu \in [-1, 1]$ and the azimuth angle $\varphi \in [0, 2\pi]$. The CFL number of transient DUGKS is set to be 0.5. Correspondingly, the characteristic line length in T-SDUGKS is set to be $l = 0.25\Delta x_{min}$ according to Eq. (10) unless otherwise stated. All computations are performed on a machine with an Intel(R) Core(TM) i7-8700 CPU @ 3.20GHz processor with 8.00 GB RAM and 64-bit operating system.

4.1. Numerical accuracy

Firstly, some general one- and two-dimensional cases are simulated to prove the accuracy of the present T-SDUGKS. The computation time and steps of the DUGKS, T-SDUGKS and R-SDUGKS are also compared here.

4.1.1. Radiation in a slab

The radiative equilibrium problem in a slab with thickness $L = 1$ is shown in Fig. 3. The left wall is kept hot with unity nondimensional emissive power ($\Phi_1 = 1$) while the right wall is kept cold with $\Phi_0 = 0$, where $\Phi = (\sigma T^4 - \sigma T_0^4) / (\sigma T_1^4 - \sigma T_0^4)$, T_0 and T_1 are the temperature of right and left walls, respectively [45], and both walls are black media. Initially, the participating medium inside the slab is cold. When the slab is filled with pure scattering media ($\omega = 1$), the solution of the problem can be expressed as [45],

$$G^*(\tau) = \frac{1}{2} \left[E_2(\tau) + \int_0^{\tau_L} G^*(\tau') E_1(|\tau - \tau'|) d\tau' \right], \quad (42)$$

where $\tau = \beta x$ is the optical path length, $\tau_L = \beta L$ is the optical thickness, and $E_n(x) = \int_0^1 t^{n-2} \exp(-x/t) dt$ is the exponential integral function. $G^* = (G - G_0) / (G_1 - G_0)$ is the nondimensional incident radiation

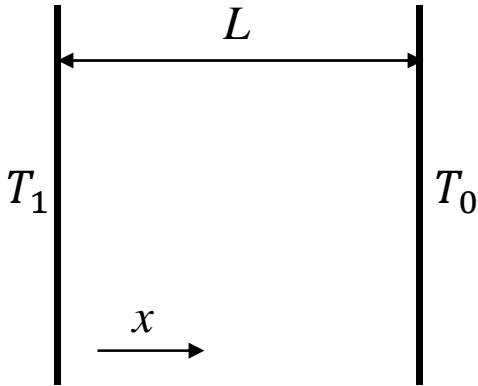


Figure 3: Schematic of one-dimensional radiation heat transfer.

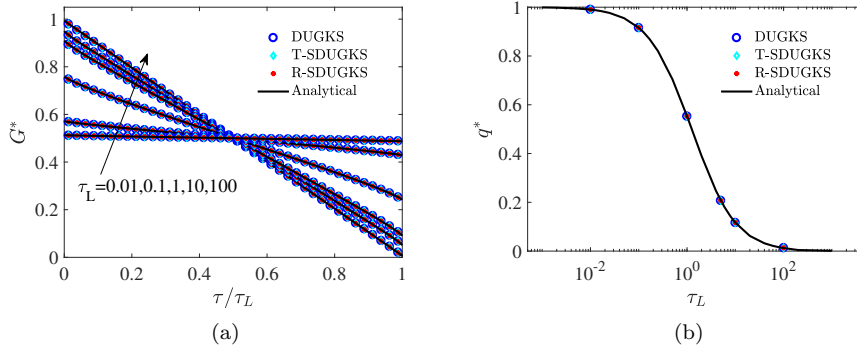


Figure 4: Radiation energy and heat flux profiles with different optical thicknesses.

energy, where $G_0 = 4\sigma T_0^4$ and $G_1 = 4\sigma T_1^4$. In fact, Eq. (42) can be numerically solved to get a “numerical exact” solution. Here we use the trapezoidal quadrature with 4000 points to solve Eq. (42), which can give mesh-independent reference solution. In our numerical simulations the angular space is discretized with the 100-point Gauss-Legendre quadrature, the physical space is discretized into $N_x = 40$ uniform cells, and the smooth reconstruction is used for the interface radiation intensity.

Figure 4 shows the distribution of nondimensional incident radiation energy G^* and heat flux q^* with the optical thickness ranging from 0.01 to 100. It can be seen that the results of DUGKS, T-SDUGKS and R-SDUGKS are all in good agreement with the analytical solutions. The computation time and steps of the three schemes are shown in Table 1, where “Rate” represents the speedup ratio in time compared to DUGKS. It can be observed that the T-SDUGKS and R-SDUGKS are much faster than the transient DUGKS for optical thin problems, but the acceleration rates decrease with increasing optical thickness, which is due to the inherent nature of the source iteration method [46].

Table 1: Comparison of the computation costs of different schemes for the slab.

τ_L	DUGKS		T-SDUGKS			R-SDUGKS		
	Time(s)	Steps	Time(s)	Steps	Rate	Time(s)	Steps	Rate
0.01	4.962	61421	0.01	98	496.2	0.009	98	551.3
0.1	0.718	8858	0.01	84	71.8	0.01	88	71.8
1	0.196	2377	0.009	67	21.8	0.006	66	32.7
5	0.289	3516	0.027	277	10.7	0.022	275	13.1
10	0.444	5458	0.07	791	6.3	0.058	786	7.7
100	3.061	37816	3.898	46616	0.8	3.3	46244	0.9

4.1.2. Radiation in a black square enclosure

In this section, the radiative heat transfer in a 2D black square enclosure of length L filled with pure scattering media is simulated. The bottom wall is kept hot ($\Phi_1 = 1$), whereas the other walls and the media are kept cold ($\Phi_0 = 0$). The schematic of the problem is shown in Fig. 5. The scatter albedo is set to be $\omega = 1$. A uniform mesh with size $N_x \times N_y = 40 \times 40$ is used. The direction cosine of zenith angle

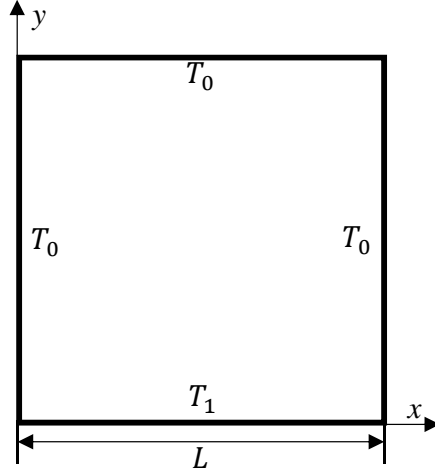


Figure 5: Schematic of two-dimensional radiation heat transfer.

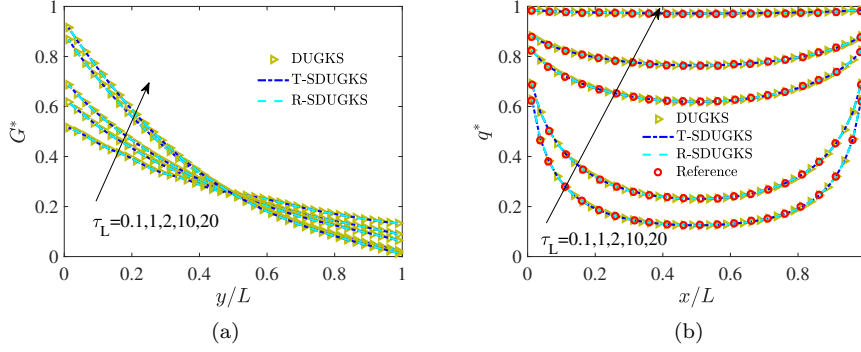


Figure 6: Radiation energy profiles along the vertical centerline and heat flux at the bottom wall with different optical thicknesses.

$\mu \in [-1, 1]$ is discretized with the 16-point Gauss-Legendre quadrature, and the azimuth angle $\varphi \in [0, \pi]$ (due to geometric symmetry) is also discretized with the 16-point Gauss-Legendre quadrature. The smooth linear interpolation is adopted when reconstructing the interface radiation intensity.

The radiation energy along the vertical centerline and heat flux at the bottom wall with different optical thicknesses are shown in Fig. 6. It can be observed from Fig. 6(b) that the results of the three DUGKS agree well with the reference results [39]. For further comparison, the radiation energy distributions from the DUGKS and T-SDUGKS are exhibited in Fig. 7. Clearly, the results predicted by the T-SDUGKS are in excellent agreement with those of the DUGKS. The computation time and steps of different methods are listed in Table 2. It can be seen that the T-SDUGKS and R-SDUGKS have faster convergence rates than the DUGKS. The comparisons show that the T-SDUGKS and R-SDUGKS are accurate and more efficient than DUGKS for steady radiative heat transfer problems.

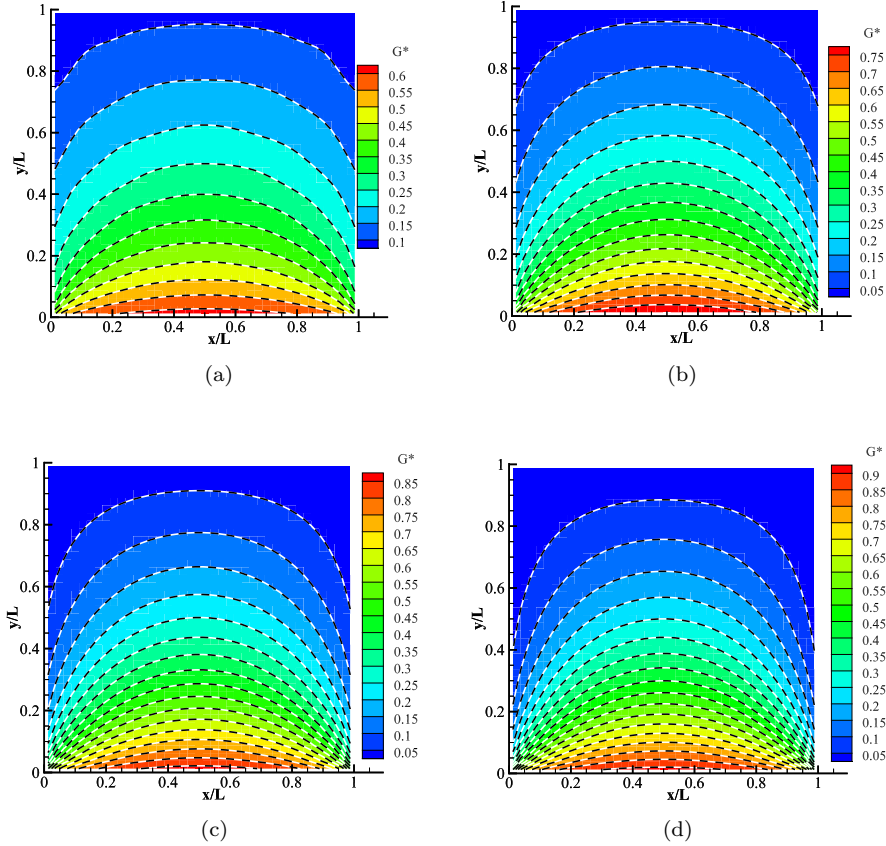


Figure 7: Radiation energy distributions in the square enclosure with different optical thicknesses.(a) $\tau = 1$, (b) $\tau = 5$, (c) $\tau = 10$ and (d) $\tau = 20$. Background: DUGKS, dashed lines: T-SDUGKS.

Table 2: Comparison of the computation costs of different schemes for the black square enclosure.

τ_L	DUGKS		T-SDUGKS			R-SDUGKS		
	Time(s)	Steps	Time(s)	Steps	Rate	Time(s)	Steps	Rate
0.1	28.066	2199	3.462	178	8.1	2.775	178	10.1
1	14.499	1099	1.868	97	7.8	1.641	97	8.8
2	15.132	1184	1.618	79	9.4	1.314	79	11.5
5	22.632	1775	2.815	151	8.0	2.382	151	9.5
10	35.353	2788	7.534	416	4.7	6.121	416	5.8
20	60.252	4759	23.011	1317	2.6	19.062	1317	3.2

4.2. Radiation in a black square enclosure with different media

The radiation in a black square enclosure filled with two different media is considered in this section. This case is used to show that the slope limiter for reconstructing the interface radiation intensity is preferred for problems with discontinuous extinction coefficients. As shown in Fig. 8, a black square with the side length of $L = 1$ is filled with two different media. The nondimensional emissive power is set to be $\Phi_1 = 1$ at the bottom wall, and $\Phi_0 = 0$ at the other walls and the media. The extinction coefficients of the inner and

outer media are β_2 and β_1 , respectively. In the simulations, the scatter albedo is set to be $\omega = 1$. β_1 ranges from 0.01 to 100 and $\beta_2 = 1/\beta_1$. In order to reduce the ray effect, the solid angle is discretized using the

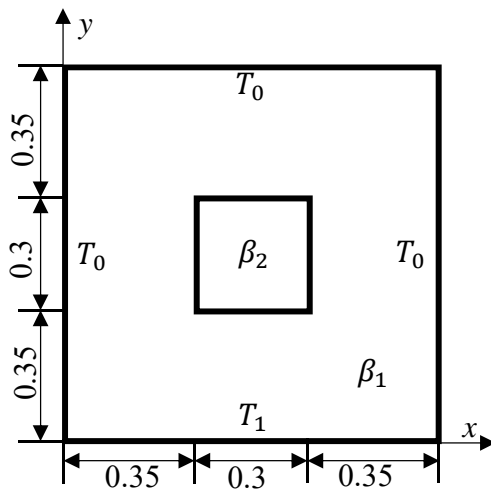


Figure 8: Schematic of two-dimensional radiation heat transfer.

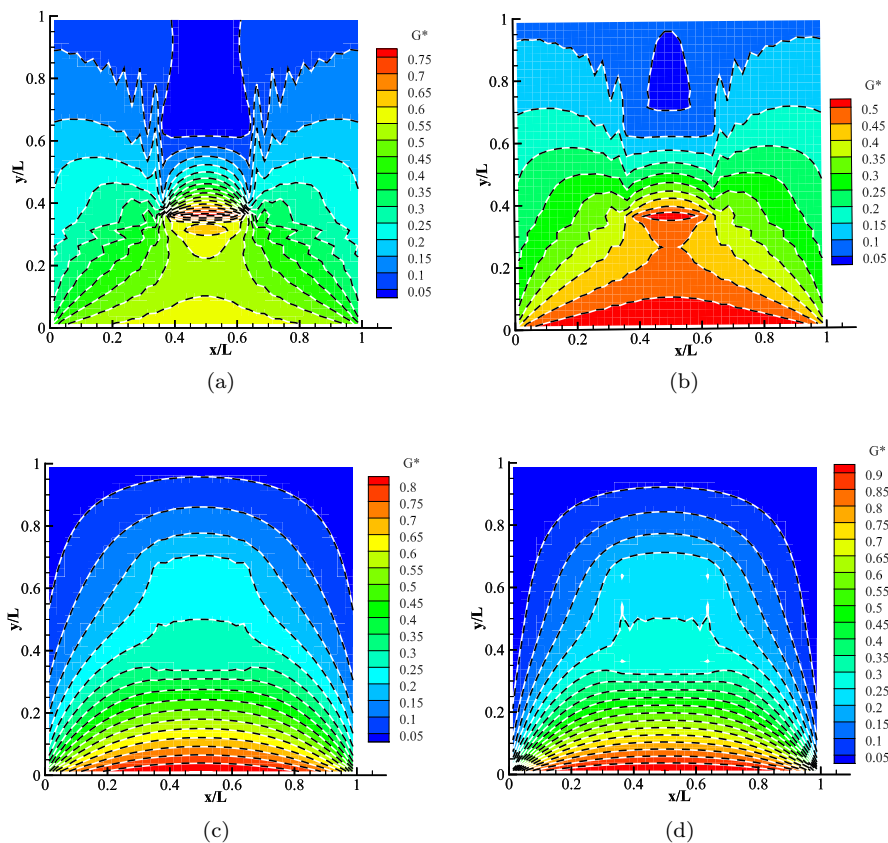


Figure 9: Radiation energy distributions in the square enclosure with smooth linear interpolation. (a) $\beta_1 = 0.01, \beta_2 = 100$, (b) $\beta_1 = 0.1, \beta_2 = 10$, (c) $\beta_1 = 10, \beta_2 = 0.1$ and (d) $\beta_1 = 100, \beta_2 = 0.01$. Background: T-SDUGKS, dashed lines: R-SDUGKS.

Gauss-Legendre quadrature with a $N_\mu \times N_\varphi = 32 \times 32$ angular mesh.

We first test the T-SDUGKS using the smooth linear reconstruction. The radiation energy with a mesh $N_x \times N_y = 40 \times 40$ is displayed in Fig. 9. Clearly, numerical oscillations appear in the optical thin area, indicating that the smooth linear interpolation is not suitable for problems with discontinuous extinction coefficients.

The T-SDUGKS using linear reconstruction with van Leer limiter is also applied to this problem. Figure 10 shows the radiation energy along the vertical centerline with different optical thicknesses and grid sizes, and Fig. 11 shows the contours of the radiation energy distributions. It can be seen that numerical oscillations disappear. From Fig. 11, it can be seen that the extinction coefficient of the inner medium has a great influence on the transport of radiation energy. When $\beta_2 > \beta_1$, a hot zone appears between the inner and outer media close to the hot wall. This can be attributed to the strong photon scattering effect of the inner optical thick medium. As $\beta_2 < \beta_1$, the thickness of the inner medium is smaller and photon scatterings are rare, leading to weak energy exchange. The above results demonstrate that the T-SDUGKS using the van Leer reconstruction is an accurate method for steady multiscale radiative heat transfer problems, while the smooth reconstruction is inappropriate for problems with discontinuous extinction coefficients.

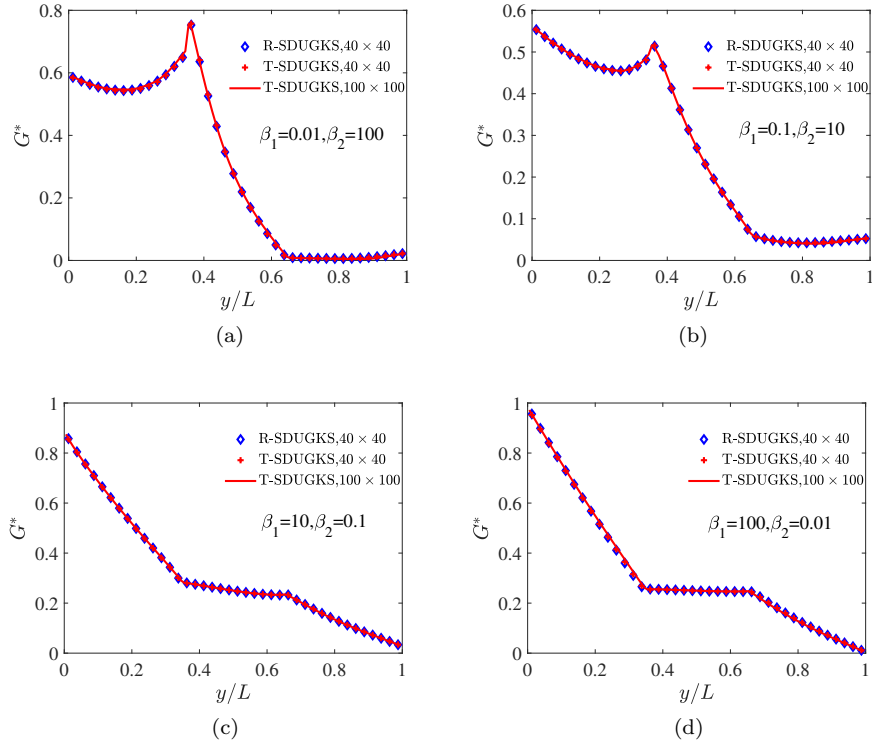


Figure 10: Radiation energy profiles along the vertical centerline with different optical thicknesses and grid sizes.

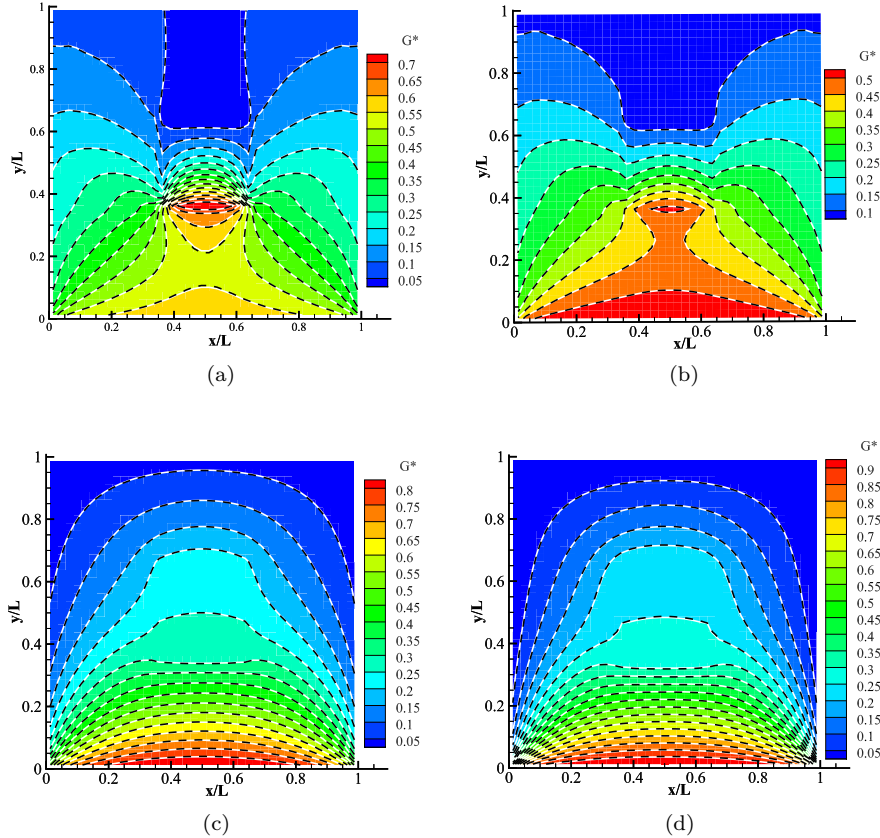


Figure 11: Radiation energy distributions in the square enclosure with van Leer limiter. (a) $\beta_1 = 0.01, \beta_2 = 100$, (b) $\beta_1 = 0.1, \beta_2 = 10$, (c) $\beta_1 = 10, \beta_2 = 0.1$ and (d) $\beta_1 = 100, \beta_2 = 0.01$. Background: T-SDUGKS, dashed lines: R-SDUGKS.

4.3. Radiation in a slab with a heat source

In this section the performance of the T-SDUGKS and the R-SDUGKS is further compared by simulating the radiation transfer in a slab of size $L = 1$ with a constant heat source, which was first considered in Ref. [37]. The transfer equation for this problem reads,

$$\mu_k \cdot \frac{dI(x, \mu_k)}{dx} = -\beta(x) I(x, \mu_k) + \frac{\beta(x)}{2} \sum_{m=1}^M I(x, \mu_m) \omega_m + \frac{\dot{Q}}{2}. \quad (43)$$

The left and right walls of the slab are kept cold with $\Phi_0 = 0$ and the heat source $\dot{Q} = 0.01$. A 40-point Gauss-Legendre quadrature is used to discretize the solid angle space, and uniform meshes with size $N_x = 40, 100, 200$ are used for the physical space, respectively. The reference solution is obtained by the DUGKS with a uniform mesh with 4000 cells.

First, we simulate the case with $\beta(x) = 100(1 + 100x^2)$. The smooth linear interpolation is adopted when reconstructing the interface radiation intensity. Figure 12 shows the radiation energy and heat flux with different meshes at $l = 0.25\Delta x$. Good agreement between the T-SDUGKS and the reference results can be observed, while significant deviations between the results of the R-SDUGKS and reference data can be found

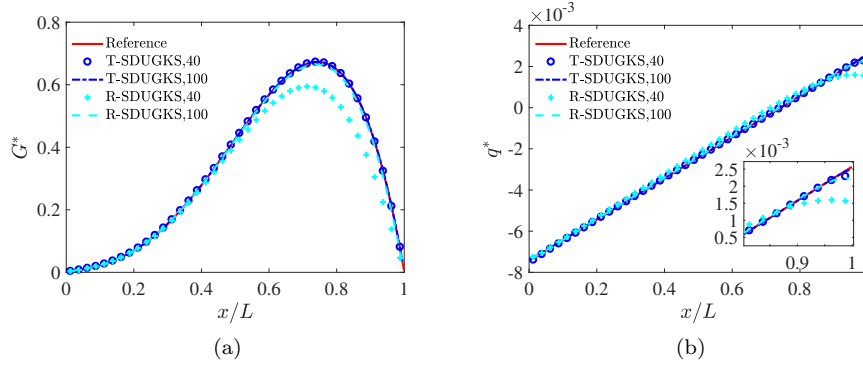


Figure 12: Radiation energy and heat flux profiles of the T-SDUGKS and R-SDUGKS with $l = 0.25dx$.

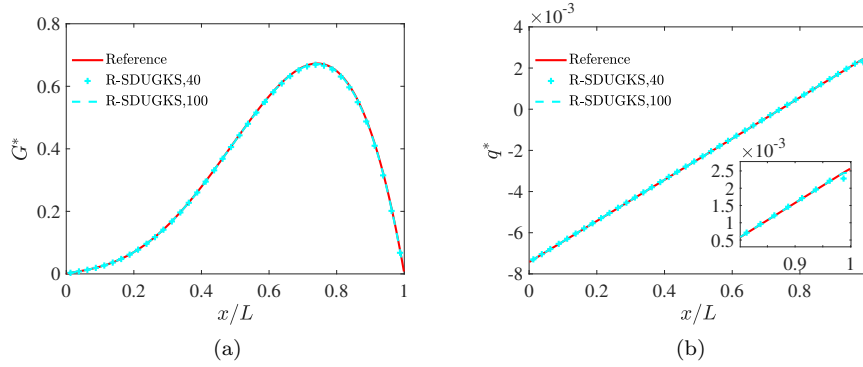


Figure 13: Radiation energy and heat flux profiles of the R-SDUGKS with $l = 1/\beta_{max}$.

with the coarse mesh ($N_x = 40$) for radiation energy and heat flux. The deviations in the R-SDUGKS may be caused by the fact that the characteristic line length is larger than $1/\beta_{max}$ [42]. Therefore, $l = 1/\beta_{max}$ is set for R-SDUGKS, which leads to a much smaller approximation error $O(l^2)$ in Eq. (37). The corresponding results are shown in Fig. 13. It is seen that the results agree well with the reference solutions, indicating that the characteristic line length in the rectangular SDUGKS is limited by the extinction coefficient, while the T-SDUGKS does not suffer from this limitation.

Furthermore, the case with a discontinuous extinction coefficient is also considered, where

$$\beta(x) = \begin{cases} 100, & 0 \leq x \leq 0.1, \\ 1000, & 0.1 < x \leq 0.5, \\ 10000, & 0.5 < x \leq 1.0. \end{cases} \quad (44)$$

The characteristic line length in T-SDUGKS is chosen to be $l = 0.25\Delta x$, while in R-SDUGKS it is chosen as $l = 1/\beta_{max}$. The van Leer limiter is adopted for this discontinuous problem. The radiation energy and heat flux are plotted in Fig. 14. It can be observed that the R-SDUGKS predicts almost incorrect results with the mesh of $N_x = 40$ while the T-SDUGKS gives the reasonable ones. With the refinement of the mesh, the results become more accurate, and the T-SDUGKS can give better results than the R-SDUGKS under the

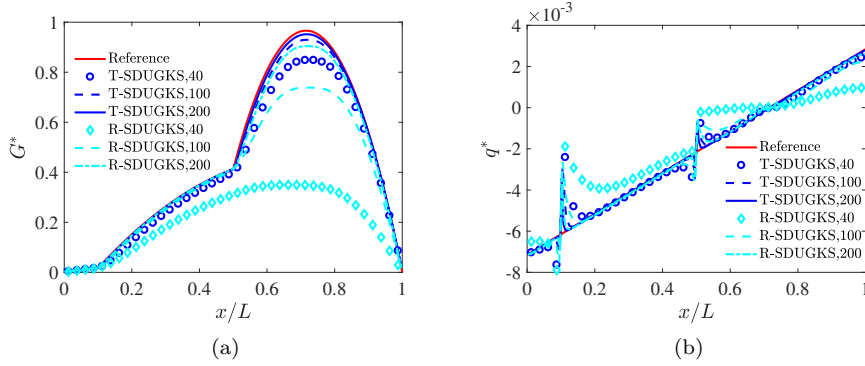


Figure 14: Radiation energy and heat flux profiles of the T-SDUGKS and R-SDUGKS.

same mesh. These results clearly demonstrate that the T-SDUGKS is more accurate and robust than the R-SDUGKS for this problem.

4.4. Radiation in a slab with large temperature gradient

The nonequilibrium radiation transport in a slab with large temperature gradient is simulated by the T-SDUGKS and DD method to test their robustness. Similar to the structure shown in Fig. 3, both the left and right walls are black media and kept clod with $\Phi_0 = 0$, and the inside participating medium is kept hot

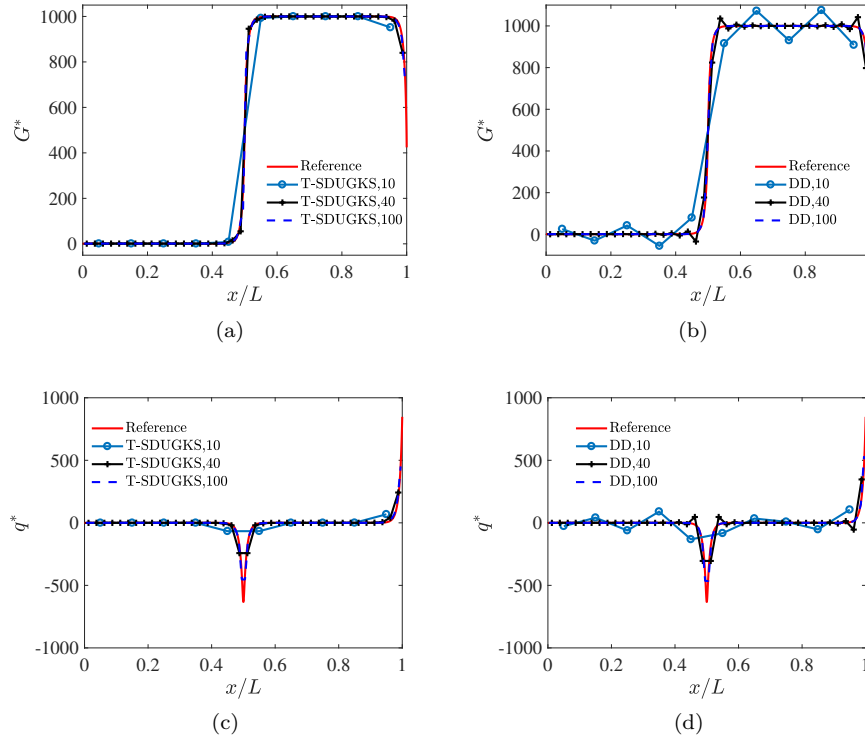


Figure 15: Radiation energy and heat flux with T-SDUGKS and DD method at $\tau_L = 100$.

with a large temperature gradient, where the emissive power inside the slab is assumed to be

$$\Phi(x) = \frac{\Phi_{max} + \Phi_{min}}{2} + \frac{\Phi_{max} - \Phi_{min}}{2} \tanh\left(\frac{x - L/2}{W}\right), \quad (45)$$

where Φ_{min} and Φ_{max} are the minimum and maximum values of emissive power in the slab, respectively. In the simulations, the scattering albedo is set to be $\omega = 0.5$, the optical thickness is set to be $\tau_L = 100, 500$, and $\Phi_{min} = 1$, $\Phi_{max} = 1000$, $W = 0.002$. The smooth linear interpolation is used in T-SDUGKS for reconstructing the interface radiation intensity. The angular space is discretized using the Gauss-Legendre quadrature with $N_\mu = 100$, and the physical space is discretized into N_x uniform cells. The DUGKS solution with 10000 uniform cells is taken as the reference solution.

Figure 15 shows the radiation energy and heat flux from T-SDUGKS and DD method at $\tau_L = 100$. It can be observed that the DD method produces nonphysical oscillations with mesh resolutions of $N_x = 10$ and 40 which can be attributed to the unresolved mean free path ($\Delta x/\lambda > 1$). On the other hand, the results given by T-SDUGKS are in good agreement with the reference solutions even with the coarsest mesh ($N_x = 10$) indicating that the mesh size is not restricted by the MFP. The results with $\tau_L = 500$ are shown in Fig. 16.

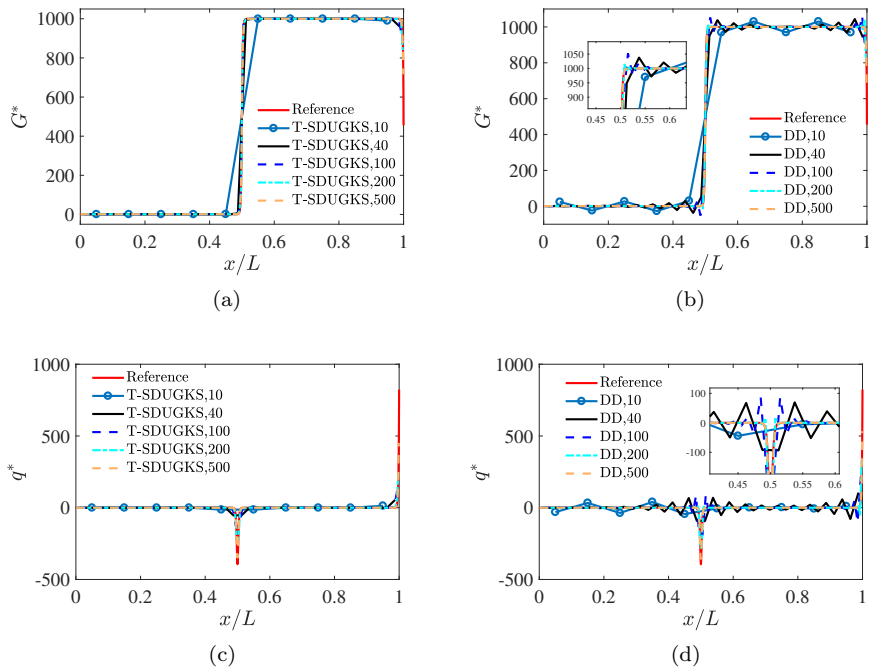


Figure 16: Radiation energy and heat flux with T-SDUGKS and DD method at $\tau_L = 500$.

It can be seen that as τ_L increases, the mesh resolution should be further increased for DD method to avoid nonphysical oscillations. The above results demonstrate that the T-SDUGKS is more stable and robust than the DD method in solving radiative heat transfer problems with large temperature gradient and optical thickness.

5. Conclusion

In this work, a steady discrete unified gas kinetic scheme using trapezoidal rule in the reconstruction of interface radiation intensity is developed for multiscale radiative heat transfer problems. With the coupling of the scattering, absorbing and emitting along the characteristic line of the RTE in determining the cell interface intensity, the T-SDUGKS can simulate multiscale radiative heat transfer problems without the limitation that the mesh size must be smaller than the photon MFP. The T-SDUGKS is validated by the one-dimensional multiscale radiation problems in a slab and two-dimensional multiscale radiation problems in a black square enclosure. Numerical results show that both the present T-SDUGKS and the original R-SDUGKS have faster convergence rates than the transient DUGKS for steady problems, especially in optical thin regions. It is also found that the present T-SDUGKS is more accurate than the R-SDUGKS, and the characteristic line length is not limited by the extinction coefficient. Furthermore, it is found that the mesh size in the T-SDUGKS is not restricted by the photon MFP, unlike the diamond difference method. In summary, the proposed T-SDUGKS is an accurate, efficient and robust scheme for steady multiscale radiative heat transfer.

The proposed T-SDUGKS is designed based on the gray and isotropic RTE model, where the frequency dependence of the intensity and anisotropic of the scattering term are ignored. The future work will extend the current method to problems with these effects.

Acknowledgments

This work was supported by the Fundamental Research Funds for the Central Universities (HUST: 2019kfyXMBZ040), the National Natural Science Foundation of China (No.12005073, No.12002131), and the China Postdoctoral Science Foundation (2021M701565).

DATA AVAILABILITY STATEMENT

The data that support the findings of this study are available from the corresponding author upon reasonable request.

References

- [1] I. M. Machado, P. Pagot, and F. M. Pereira, "Experimental study of radiative heat transfer from laminar non-premixed methane flames diluted with CO_2 and N_2 ," International Journal of Heat and Mass Transfer, vol. 158, p. 119984, 2020.
- [2] A. Gunnarsson, K. Andersson, B. R. Adams, and C. Fredriksson, "Full-scale 3d-modelling of the radiative heat transfer in rotary kilns with a present bed material," International Journal of Heat and Mass Transfer, vol. 147, p. 118924, 2020.

- [3] B. Hunter and Z. Guo, “Normalization of various phase functions for radiative heat transfer analysis in a solar absorber tube,” Heat transfer engineering, vol. 35, no. 6-8, pp. 791–801, 2014.
- [4] W. Fuqiang, M. Lanxin, C. Ziming, T. Jianyu, H. Xing, and L. Linhua, “Radiative heat transfer in solar thermochemical particle reactor: a comprehensive review,” Renewable and Sustainable Energy Reviews, vol. 73, pp. 935–949, 2017.
- [5] M. Chahlaoui, F. Bellet, F. Fichot, and J. Taine, “Radiative transfer within non beerian porous media with semitransparent and opaque phases in non equilibrium: Application to reflooding of a nuclear reactor,” International journal of heat and mass transfer, vol. 55, no. 13-14, pp. 3666–3676, 2012.
- [6] K.-N. Liou, An introduction to atmospheric radiation. Elsevier, 2002.
- [7] J. Huang, C. Lin, Y. Li, and B. Huang, “Effects of humidity, aerosol, and cloud on subambient radiative cooling,” International Journal of Heat and Mass Transfer, vol. 186, p. 122438, 2022.
- [8] A. Broc, V. Joly, J.-P. Lafon, and C. Marmignon, “Nonequilibrium radiative hypersonic flows: aerospace applications,” Astrophysics and space science, vol. 260, no. 1, pp. 29–43, 1998.
- [9] J. Shang and S. Surzhikov, “Nonequilibrium radiative hypersonic flow simulation,” Progress in Aerospace Sciences, vol. 53, pp. 46–65, 2012.
- [10] D. Gorpas, D. Yova, and K. Politopoulos, “A three-dimensional finite elements approach for the coupled radiative transfer equation and diffusion approximation modeling in fluorescence imaging,” Journal of Quantitative Spectroscopy and Radiative Transfer, vol. 111, no. 4, pp. 553–568, 2010.
- [11] Z. M. Zhang, Z. M. Zhang, and Luby, Nano/microscale heat transfer, vol. 410. Springer, 2007.
- [12] M. F. Modest, Radiative heat transfer. Academic press, 2013.
- [13] M. Roger, C. Caliot, N. Crouseilles, and P. Coelho, “A hybrid transport-diffusion model for radiative transfer in absorbing and scattering media,” Journal of Computational Physics, vol. 275, pp. 346–362, 2014.
- [14] J. R. Howell, “Application of monte carlo to heat transfer problems,” in Advances in heat transfer, vol. 5, pp. 1–54, Elsevier, 1969.
- [15] R. Y. Rubinstein and D. P. Kroese, Simulation and the Monte Carlo method. John Wiley & Sons, 2016.
- [16] Truelove and S. J., “Discrete-ordinate solutions of the radiation transport equation,” Journal of Heat Transfer, vol. 109:4, no. 4, pp. 1048–1051, 1987.

- [17] R.-R. Zhou and B.-W. Li, “The modified discrete ordinates method for radiative heat transfer in two-dimensional cylindrical medium,” International Journal of Heat and Mass Transfer, vol. 139, pp. 1018–1030, 2019.
- [18] H. Grissa, F. Askri, M. B. Salah, and S. B. Nasrallah, “Three-dimensional radiative transfer modeling using the control volume finite element method,” Journal of Quantitative Spectroscopy and Radiative Transfer, vol. 105, no. 3, pp. 388–404, 2007.
- [19] G. D. Raithby and E. H. Chui, “A finite-volume method for predicting a radiant heat transfer in enclosures with participating media,” Asme Transactions Journal of Heat Transfer, vol. 112, no. 2, 1990.
- [20] G. Raithby, “Discussion of the finite-volume method for radiation, and its application using 3d unstructured meshes,” Numerical Heat Transfer: Part B: Fundamentals, vol. 35, no. 4, pp. 389–405, 1999.
- [21] J. Zhao and L. Liu, “Solution of radiative heat transfer in graded index media by least square spectral element method,” International Journal of Heat and Mass Transfer, vol. 50, no. 13-14, pp. 2634–2642, 2007.
- [22] H. Hottel and E. Cohen, “Radiant heat exchange in a gas-filled enclosure: Allowance for nonuniformity of gas temperature,” AIChE Journal, vol. 4, no. 1, pp. 3–14, 1958.
- [23] J. C. Henson and W. Malalasekera, “Comparison of the discrete transfer and monte carlo methods for radiative heat transfer in three-dimensional nonhomogeneous scattering media,” Numerical Heat Transfer, Part A Applications, vol. 32, no. 1, pp. 19–36, 1997.
- [24] S. H. Sarvari, “Solution of multi-dimensional radiative heat transfer in graded index media using the discrete transfer method,” International Journal of Heat and Mass Transfer, vol. 112, pp. 1098–1112, 2017.
- [25] H.-C. Zhou, D.-L. Chen, and Q. Cheng, “A new way to calculate radiative intensity and solve radiative transfer equation through using the monte carlo method,” Journal of Quantitative Spectroscopy and Radiative Transfer, vol. 83, no. 3-4, pp. 459–481, 2004.
- [26] Z. Huang, H. Zhou, Q. Cheng, and P.-f. Hsu, “Solution of radiative intensity with high directional resolution in three-dimensional rectangular enclosures by dresor method,” International Journal of Heat and Mass Transfer, vol. 60, pp. 81–87, 2013.
- [27] F. A. Kulacki, S. Acharya, Y. Chudnovsky, R. M. Cotta, R. Devireddy, V. K. Dhir, M. P. Mengüç, J. Mostaghimi, and K. Vafai, Handbook of thermal science and engineering. Springer, 2018.
- [28] J. R. Howell, M. P. Mengüç, K. Daun, and R. Siegel, Thermal radiation heat transfer. CRC press, 2020.

- [29] D. Wang and H. Zhou, “Quantitative evaluation of the computational accuracy for the monte carlo calculation of radiative heat transfer,” Journal of Quantitative Spectroscopy and Radiative Transfer, vol. 226, pp. 100–114, 2019.
- [30] F. Golse, S. Jin, and C. D. Levermore, “A domain decomposition analysis for a two-scale linear transport problem,” ESAIM: Mathematical Modelling and Numerical Analysis, vol. 37, no. 6, pp. 869–892, 2003.
- [31] M. Roger and N. Crouseilles, “A dynamic multi-scale model for transient radiative transfer calculations,” Journal of Quantitative Spectroscopy and Radiative Transfer, vol. 116, pp. 110–121, 2013.
- [32] P. J. Coelho, N. Crouseilles, P. Pereira, and M. Roger, “Multi-scale methods for the solution of the radiative transfer equation,” Journal of Quantitative Spectroscopy and Radiative Transfer, vol. 172, pp. 36–49, 2016.
- [33] K. Xu and J.-C. Huang, “A unified gas-kinetic scheme for continuum and rarefied flows,” Journal of Computational Physics, vol. 229, no. 20, pp. 7747–7764, 2010.
- [34] Y. Zhu and K. Xu, “The first decade of unified gas kinetic scheme,” arXiv preprint arXiv:2102.01261, 2021.
- [35] Z. Guo, K. Xu, and R. Wang, “Discrete unified gas kinetic scheme for all knudsen number flows: Low-speed isothermal case,” Physical Review E, vol. 88, no. 3, p. 033305, 2013.
- [36] Z. Guo and K. Xu, “Progress of discrete unified gas-kinetic scheme for multiscale flows,” Advances in Aerodynamics, vol. 3, no. 1, pp. 1–42, 2021.
- [37] L. Mieussens, “On the asymptotic preserving property of the unified gas kinetic scheme for the diffusion limit of linear kinetic models,” Journal of Computational Physics, vol. 253, pp. 138–156, 2013.
- [38] W. Sun, S. Jiang, and K. Xu, “An asymptotic preserving unified gas kinetic scheme for gray radiative transfer equations,” Journal of Computational Physics, vol. 285, pp. 265–279, 2015.
- [39] X.-P. Luo, C.-H. Wang, Y. Zhang, H.-L. Yi, and H.-P. Tan, “Multiscale solutions of radiative heat transfer by the discrete unified gas kinetic scheme,” Physical Review E, vol. 97, no. 6, p. 063302, 2018.
- [40] X. Song, C. Zhang, X. Zhou, and Z. Guo, “Discrete unified gas kinetic scheme for multiscale anisotropic radiative heat transfer,” Advances in Aerodynamics, vol. 2, no. 1, pp. 1–15, 2020.
- [41] Y. Shi, W. Sun, L. Li, and P. Song, “An improved unified gas kinetic particle method for radiative transfer equations,” Journal of Quantitative Spectroscopy and Radiative Transfer, vol. 261, p. 107428, 2021.

- [42] X. Zhou and Z. Guo, “Discrete unified gas kinetic scheme for steady multiscale neutron transport,” Journal of Computational Physics, vol. 423, p. 109767, 2020.
- [43] B. Van Leer, “Towards the ultimate conservative difference scheme. iv. a new approach to numerical convection,” Journal of computational physics, vol. 23, no. 3, pp. 276–299, 1977.
- [44] M. Abramowitz and I. A. Stegun, Handbook of mathematical functions with formulas, graphs, and mathematical tables, vol. 55. US Government printing office, 1972.
- [45] M. A. Heaslet and R. F. Warming, “Radiative transport and wall temperature slip in an absorbing planar medium,” International Journal of Heat and Mass Transfer, vol. 8, no. 7, pp. 979–994, 1965.
- [46] M. L. Adams and E. W. Larsen, “Fast iterative methods for discrete-ordinates particle transport calculations,” Progress in nuclear energy, vol. 40, no. 1, pp. 3–159, 2002.